mathematics

Article

The Concept of Topological Derivative for Eigenvalue Optimization Problem for Plane Structures

Fernando Soares Carvalho [1,*] and Carla Tatiana Mota Anflor [2,†]

[1] Department of Mathematics, Federal University of Tocantins, Palmas 77650-000, Brazil
[2] Group of Experimental and Computational Mechanics, University of Brasilia, Brasilia 70910-900, Brazil; anflor@unb.br
* Correspondence: fscarvalho@uft.edu.br
† Current address: Arraias 77330-000, Brazil.

Abstract: This paper presents the topological derivative of the first eigenvalue for the free vibration model of plane structures. We conduct a topological asymptotic analysis to account for perturbations in the domain caused by inserting a small inclusion. The paper includes a rigorous derivation of the topological derivative for the eigenvalue problem along with a proof of its existence. Additionally, we provide numerical examples that illustrate the application of the proposed methodology for maximizing the first eigenvalue in plane structures. The results demonstrate that multiple eigenvalues were not encountered.

Keywords: optimal design of plane structures; topological derivative; first eigenvalue maximization

MSC: 35A25

check for updates

Citation: Carvalho, F.S.; Anflor, C.T.M. The Concept of Topological Derivative for Eigenvalue Optimization Problem for Plane Structures. *Mathematics* **2024**, *12*, 2762. https://doi.org/10.3390/math12172762

Academic Editors: Kai Zhang and Piyang Liu

Received: 18 June 2024
Revised: 30 August 2024
Accepted: 3 September 2024
Published: 6 September 2024

Copyright: © 2024 by the authors. Licensee MDPI, Basel, Switzerland. This article is an open access article distributed under the terms and conditions of the Creative Commons Attribution (CC BY) license (https://creativecommons.org/licenses/by/4.0/).

1. Introduction

Some considerations such as dynamic response and loads are important for understanding the behavior and design of structures. Structures under dynamic analysis are governed by linear differential equations, which involve solving an eigenvalue problem. The eigenvalue problem is crucial in many real-world applications, particularly in structural optimization, as it significantly contributes to structural integrity. When the excitation frequency matches one of the natural frequencies of vibration, the structure becomes highly responsive, which can lead to damage or collapse. Structural behavior is affected when variations in system parameters lead to changes in eigenvalues; eigenvectors; and, consequently, the final response characteristics of the system. The magnitude of these variations is reflected in the derivatives of the system's eigenvalues and eigenvectors. One of the main concerns of sensitivity analysis is the presence of multiple eigenvalues. During the topology optimization process, only simple eigenvalues are present in the initial steps. However, as the iterative process progresses and the geometry changes, multiple eigenvalues may appear. The presence of multiple eigenvalues leads to convergence issues in optimization algorithms because they are not differentiable in the common sense [1,2]. Since then, several methods have been proposed to avoid the presence of multiple eigenvalues [3–6]. The conventional notion of derivative is naturally extended to functionals through the concept of the topological derivative (D_T), where the variable is a geometric domain subject to singular topology changes.

Concerning structural topology optimization, the D_T provides the exact sensitivity of the associated objective functionals due to perturbations such as the insertion of infinitesimal voids, inclusions, or even cracks. In particular, for dynamic problems, the D_T for simple eigenvalues of the Laplacian was considered by [7], and for multiple eigenvalues in elasticity problems by [8]. A similar work concerning the augmented Lagrangian method based on the concept of the topological derivative was also addressed by [9], where numerical results considering compliance and eigenfrequency constraints were introduced by the authors. More recently, the D_T of L^2 and energy norms associated with the solution to plate bending, considering both Kirchhoff and Reissner–Mindlin theories, was introduced by [10]. In addition to the maximization of the first eigenvalue, the sensitivities obtained were adapted to the context of plate topology optimization for plates under elastic support and free vibration conditions. In [11], the D_T was derived for membrane eigenvalue maximization concerning the nucleation of inclusions endowed with different material properties from the background. According to the numerical results, the presence of multiple eigenvalues was not observed as the iterative process evolved, even as the geometry became complex.

The field of eigenvalue topology optimization remains significant and requires the development of new methodologies. These should incorporate classical techniques such as sensitivity analysis, level set methods, and the bubble method, among others, to effectively address various challenges. Ref. [12] introduced a phase field-based structural optimization method that simplifies computation and improves efficiency compared to traditional level-set methods. This method uses a phase field function and solves a time-dependent reaction–diffusion equation but relies on the initial shape and requires careful management of perimeter control effects. More recently, ref. [13] presented an enhanced phase field method with multi-level correction, which improves accuracy and reduces computational costs for eigenfrequency topology optimization, as demonstrated by numerical examples in 2D and 3D.

As mentioned earlier, eigenfrequency optimization is a prominent research topic. The present work revisits the subject discussed in [11] to incorporate the problem of plane structures. The focus is on deriving the D_T for maximizing the first eigenvalue. A closed formula for the D_T of the first eigenvalue for plane structures is obtained. The resulting formula is used together with a level-set domain representation method to develop a topology design algorithm, as implemented in [14]. The optimal topology for the plane structure under prescribed boundary conditions is achieved by maximizing the first eigenvalue while minimizing the volume. Several proposed numerical examples demonstrate the feasibility of the present methodology in addressing topology optimizations. It is worth mentioning that, to the authors' knowledge, the concept of D_T for the eigenvalue problem for plane structures, considering mathematical rigor, has not been addressed elsewhere. Additionally, several numerical examples are explored. This paper is organized as follows. The topological derivative for plane structure problems is introduced in Section 2. In Section 3, some numerical examples are presented, showing that the D_T derived here successfully solves eigenvalue problems for plane structures. Finally, the conclusions are summarized in Section 4.

2. Topological Derivative

Consider, for instance, an open and bounded domain $\Omega \subset R^2$ such that it is subject to a nonsmooth perturbation confined in a small ball $B_\varepsilon(\hat{x})$ of radius ε and center at $\hat{x} \in \Omega$,

$$\psi(\chi_\varepsilon(\hat{x})) = \psi(\chi) + f(\varepsilon)D_T\psi(\hat{x}) + o(f(\varepsilon)), \tag{1}$$

where $\psi(\chi)$ is the shape functional associated with the unperturbed domain, $f(\varepsilon)$ is a positive first-order correction function of ψ, and $o(f(\varepsilon))$ is the remainder, such that $o(f(\varepsilon))/f(\varepsilon) \to 0$ as $\varepsilon \to 0$. The function χ is the characteristic function associated with the unperturbed domain, and χ_ε is the characteristic function associated with the perturbed domain. The function $\hat{x} \mapsto D_T\psi(\hat{x})$ is termed the topological derivative of ψ at $\hat{x}$. The domain Ω is then divided into two subdomains, $\omega \subset \Omega$ and its complement $\Omega \setminus \omega$. Finally, a set of piecewise constant functions α, ρ, and β (which are the contrasts in the material properties) is considered and introduced according to Table 1.

Table 1. Values of α, ρ, and β.

	$\boldsymbol{\alpha}$	$\boldsymbol{\rho}$	$\boldsymbol{\beta}$
$\Omega \setminus \omega$	α_0	ρ_0	β_0
ω	α_1	ρ_1	β_1

The topological perturbation results from the nucleation of a small circular inclusion of the form $\omega_\varepsilon(\widehat{x}) := B_\varepsilon(\widehat{x}) = |x - \widehat{x}| < \varepsilon$ for $\widehat{x} \in \Omega$. In this specific case, the perturbation is governed by a set of piecewise constant functions α_ε, ρ_ε, and β_ε, as introduced in Tables 2 and 3.

Table 2. Values of α_ε, ρ_ε, and β_ε.

	$\boldsymbol{\alpha_\varepsilon}$	$\boldsymbol{\rho_\varepsilon}$	$\boldsymbol{\beta_\varepsilon}$
$\Omega \setminus B_\varepsilon$	α	ρ	β
B_ε	$\gamma_\alpha \alpha$	$\gamma_\rho \rho$	$\gamma_\beta \beta$

Table 3. Values of γ_α, γ_ρ, and γ_β.

	$\boldsymbol{\gamma_\alpha}$	$\boldsymbol{\gamma_\rho}$	$\boldsymbol{\gamma_\beta}$
$\Omega \setminus \omega$	α_1/α_0	ρ_1/ρ_0	β_1/β_0
ω	α_0/α_1	ρ_0/ρ_1	β_0/β_1

2.1. Plane Structures

This section introduces the mathematical model for the plane structure problem and the shape functionals previously introduced herein in relation to the eigenvalue problem, for the sake of completeness. It also covers both the perturbed and unperturbed problems and demonstrates the existence of the associated topological derivative.

The original unperturbed problem can be stated as follows: Find $u \in \mathcal{V}(\Omega)$, such that

$$\int_\Omega \alpha \sigma(\boldsymbol{u}) \cdot \nabla^s \boldsymbol{v} + \int_\Omega \rho k \boldsymbol{u} \cdot \boldsymbol{v} = \int_\Omega \beta \boldsymbol{f} \cdot \boldsymbol{v} \quad \forall \boldsymbol{v} \in \mathcal{V}(\Omega), \tag{2}$$

where $\mathcal{V}(\Omega) = H_0^1(\Omega; R^2)$. The coefficients α, ρ, and $\beta \in \mathbb{R}^+$, are given in Table 1. In addition, $\sigma(\boldsymbol{u}) = \mathbb{C}\nabla^s \boldsymbol{u}$, $\boldsymbol{u} : \Omega \mapsto R^2$ is the displacement field and k is a positive function. The symmetric part of the displacement gradient tensor $\nabla^s \boldsymbol{u}$ and constitutive tensor $\mathbb{C}$ are given by

$$\nabla^s \boldsymbol{u} = \frac{\nabla \boldsymbol{u} + (\nabla \boldsymbol{u})^T}{2} \quad \text{and} \quad \mathbb{C} = \frac{E}{1+\nu}\left(\mathbb{I} + \frac{\nu}{1-\nu}\mathbf{I} \otimes \mathbf{I}\right), \tag{3}$$

where the symbols I and $\mathbb{I}$ represent the second- and fourth-order identity tensors, respectively. It is worth mentioning that only the homogeneous Dirichlet condition on the boundary $\partial\Omega$ was considered. However, this could be replaced by any other boundary condition, provided the problem of interest remains well-posed.

Additionally, ν is the Poisson ratio and E is the Young's modulus. The L^2 and energy norm shape functionals we are dealing with are defined as follows:

$$\mathcal{G}(u) = \int_\Omega \rho k \|\boldsymbol{u}\|^2 \qquad \text{and} \qquad \mathcal{J}(u) = \int_\Omega \alpha \sigma(\boldsymbol{u}) \cdot \nabla^s \boldsymbol{u}. \tag{4}$$

To simplify the expression of the topological derivatives, we introduce the adjoint problems for displacements q and p as follows:

$$q \in \mathcal{V}(\Omega) : \int_\Omega \alpha \sigma(\boldsymbol{q}) \cdot \nabla^s \boldsymbol{v} + \int_\Omega \rho k \boldsymbol{q} \cdot \boldsymbol{v} = -2\int_\Omega \rho k \boldsymbol{u} \cdot \boldsymbol{v}, \quad \forall \boldsymbol{v} \in \mathcal{V}(\Omega), \tag{5}$$

$$p \in \mathcal{V}(\Omega) : \int_\Omega \alpha\sigma(\boldsymbol{p}) \cdot \nabla^s \boldsymbol{v} + \int_\Omega \rho k \boldsymbol{p} \cdot \boldsymbol{v} = -2\int_\Omega \alpha\sigma(\boldsymbol{u}) \cdot \nabla^s \boldsymbol{v}, \quad \forall \boldsymbol{v} \in \mathcal{V}(\Omega). \tag{6}$$

The topologically perturbed counterpart of problem (2) is expressed as follows: Find $\boldsymbol{u}_\varepsilon \in \mathcal{V}(\Omega)$, such that

$$\int_\Omega \alpha_\varepsilon \sigma(\boldsymbol{u}_\varepsilon) \cdot \nabla^s \boldsymbol{v} + \int_\Omega \rho_\varepsilon k \boldsymbol{u}_\varepsilon \cdot \boldsymbol{v} = \int_\Omega \beta_\varepsilon \boldsymbol{f} \cdot \boldsymbol{v} \quad \forall \boldsymbol{v} \in \mathcal{V}(\Omega), \tag{7}$$

where the coefficients α_ε, ρ_ε, and β_ε are defined through Tables 2 and 3. The associated shape functionals are then defined as

$$\mathcal{G}_\varepsilon(u_\varepsilon) = \int_\Omega \rho_\varepsilon k \|\boldsymbol{u}_\varepsilon\|^2 \qquad \text{and} \qquad \mathcal{J}_\varepsilon(u_\varepsilon) = \int_\Omega \alpha_\varepsilon \sigma(\boldsymbol{u}_\varepsilon) \cdot \nabla^s \boldsymbol{u}_\varepsilon. \tag{8}$$

2.1.1. Existence of the Topological Derivative

Equations (2) and (7) introduce the shape functionals for the original and perturbed domains. Based on these, the existence of the associated topological derivative can be stated as follows:

Lemma 1. *Let u and u_ε be solutions to the original (2) and perturbed (7) problems, respectively. Then, the estimate $\|\boldsymbol{u}_\varepsilon - \boldsymbol{u}\|_{H^1(\Omega;R^2)} = O(\varepsilon)$ holds true.*

Proof. Let us subtract (2) from (7). By setting $\boldsymbol{v} = \boldsymbol{u}_\varepsilon - \boldsymbol{u}$ as the test function, after some simple analytical work, there is

$$\begin{aligned}\int_\Omega \alpha_\varepsilon \sigma(\boldsymbol{u}_\varepsilon - \boldsymbol{u}) \cdot \nabla^s(\boldsymbol{u}_\varepsilon - \boldsymbol{u}) + \int_\Omega \rho_\varepsilon k \|\boldsymbol{u}_\varepsilon - \boldsymbol{u}\|^2 = \\ \int_{B_\varepsilon} (1-\gamma_\alpha)\alpha\sigma(\boldsymbol{u}) \cdot \nabla^s(\boldsymbol{u}_\varepsilon - \boldsymbol{u}) + \int_{B_\varepsilon} (1-\gamma_\rho)\rho k \boldsymbol{u} \cdot (\boldsymbol{u}_\varepsilon - \boldsymbol{u}) \\ - \int_{B_\varepsilon} (1-\gamma_\beta)\beta \boldsymbol{f} \cdot (\boldsymbol{u}_\varepsilon - \boldsymbol{u}),\end{aligned} \tag{9}$$

where the contrasts introduced in Tables 2 and 3 are considered. The Cauchy–Schwarz inequality yields

$$\int_\Omega \alpha_\varepsilon \sigma(\boldsymbol{u}_\varepsilon - \boldsymbol{u}) \cdot \nabla^s(\boldsymbol{u}_\varepsilon - \boldsymbol{u}) + \int_\Omega \rho_\varepsilon k \|\boldsymbol{u}_\varepsilon - \boldsymbol{u}\|^2 \leqslant C_1 \varepsilon \|\boldsymbol{u}_\varepsilon - \boldsymbol{u}\|_{H^1(\Omega;R^2)}, \tag{10}$$

where the elliptic regularity of function u is used. The coercivity of the bilinear form on the left-hand side of Equation (10) results

$$c\|\boldsymbol{u}_\varepsilon - \boldsymbol{u}\|^2_{H^1(\Omega;R^2)} \leqslant \int_\Omega \alpha_\varepsilon \sigma(\boldsymbol{u}_\varepsilon - \boldsymbol{u}) \cdot \nabla^s(\boldsymbol{u}_\varepsilon - \boldsymbol{u}) + \int_\Omega \rho_\varepsilon k \|\boldsymbol{u}_\varepsilon - \boldsymbol{u}\|^2 \tag{11}$$

which leads to the result

$$\|\boldsymbol{u}_\varepsilon - \boldsymbol{u}\|_{H^1(\Omega;R^2)} \leqslant C\varepsilon, \tag{12}$$

with the constant $C = C_1/c$ independent of the small parameter ε. □

2.1.2. Topological Sensitivities

The following fourth-order polarization tensor associated with the elasticity model is introduced as

$$\mathbb{P} = \frac{1}{2}\frac{1-\gamma_\alpha}{1+\gamma_\alpha\delta_2}\left((1-\delta_2)\mathbb{I} + \frac{1}{2}(\delta_1-\delta_2)\frac{1-\gamma_\alpha}{1+\gamma_\alpha\delta_1}\mathbf{I}\otimes\mathbf{I}\right). \tag{13}$$

The constants δ_1 and δ_2 are given by

$$\delta_1 = \frac{\mu_l + \lambda_l}{\mu_l}, \qquad \delta_2 = \frac{3\mu_l + \lambda_l}{\mu_l + \lambda_l}, \tag{14}$$

where μ_l and λ_l are Lame's coefficients, both considered constants everywhere. In this case, the plane stress assumption is applied as

$$\mu_l = \frac{E}{2(1+\nu)} \qquad \lambda_l = \frac{\nu E}{1-\nu^2}. \tag{15}$$

The two main results of this section are stated here and are analogous to the work of [11]. The proofs of Theorems 1 and 2 are in the Appendix A.

Theorem 1. *Let $\mathcal{G}(u)$ be the shape functional defined by (4)-left; then, its associated topological derivative is given by*

$$D_T\mathcal{G} = \alpha\mathbb{P}\sigma(\boldsymbol{u}) \cdot \nabla^s \boldsymbol{q} - (1-\gamma_\rho)\rho k \boldsymbol{u} \cdot (\boldsymbol{u} + \boldsymbol{q}) + (1-\gamma_\beta)\beta \boldsymbol{f} \cdot \boldsymbol{q} \quad \text{a.e. in } \Omega \tag{16}$$

where $\boldsymbol{q}$ is the adjoint state solution of (5).

Theorem 2. *Let $\mathcal{J}(u)$ be the shape functional presented in (4)-right; then, its topological derivative is given by*

$$D_T\mathcal{J} = \alpha\mathbb{P}\sigma(\boldsymbol{u}) \cdot \nabla^s (\boldsymbol{u} + \boldsymbol{p}) - (1-\gamma_\rho)\rho k \boldsymbol{u} \cdot \boldsymbol{p} + (1-\gamma_\beta)\beta \boldsymbol{f} \cdot \boldsymbol{p} \quad \text{a.e. in } \Omega \tag{17}$$

where $\boldsymbol{p}$ is the adjoint solution of problem (6).

2.2. Eigenvalue Problem

The eigenvalue problem for the plane structures model of clamped free vibration can be stated as follows: Find u and λ, such that

$$\begin{cases} -\operatorname{div}(\alpha\sigma(\boldsymbol{u})) &= \lambda\rho\boldsymbol{u} \quad \text{in} \quad \Omega, \\ \boldsymbol{u} &= 0 \quad \text{on} \quad \partial\Omega. \end{cases} \tag{18}$$

One can define the associated first eigenvalue as

$$\lambda_1 = \inf_{\boldsymbol{u} \in H_0^1(\Omega;\mathbb{R}^2),\, \boldsymbol{u} \neq 0} \frac{\int_\Omega \alpha\sigma(\boldsymbol{u}) \cdot \nabla^s \boldsymbol{u}}{\int_\Omega \rho \|\boldsymbol{u}\|^2}, \tag{19}$$

with u being the solution of (18).

Note that D_T obeys the quotient rule for differentiation and uses the functions described in Theorems 1 and 2. In particular, since the topological derivative obeys the basic rules of the differential calculus (including the quotient rule for differentiation), the rigorous justification for these kind of results can be found in the book by [15] (Ch 9). The topological derivative of

$$J(\mathcal{D}) := \lambda_1, \tag{20}$$

is given by

$$D_T J = \frac{-\alpha\mathbb{P}\sigma(\boldsymbol{u}) \cdot \nabla^s \boldsymbol{u} + (1-\gamma_\rho)\rho\lambda_1\|\boldsymbol{u}\|^2}{\int_\Omega \rho\|\boldsymbol{u}\|^2}. \tag{21}$$

3. Numerical Results

In this section, several numerical examples are presented to demonstrate the capability of the topological derivative concept in delivering optimal topologies for the problems addressed here. Based on the results from the numerical examples presented, the effectiveness of the proposed methodology for optimizing the first eigenvalue under various boundary conditions and loading scenarios will be evaluated.

In all examples, the topological optimization problem focuses on maximizing the first eigenvalue while adhering to a volume constraint. The convergence to a local minimum is demonstrated through various numerical examples. We apply a topology optimization algorithm that employs an evolution equation for the level-set function, based on D_T (for further details, see [14]).

First Eigenvalue Maximization

Three cases are presented: Cases A, B, and C. We introduce a hold-all domain $\mathcal{D} \subset R^2$ such that $\Omega \subseteq \mathcal{D}$. The hold-all domain is discretized using linear triangular finite elements, resulting in an initial grid with uniform mesh spacing.

In Case A, the hold-all domain $\mathcal{D}$ is a rectangle $(0,3) \times (0,1), \mathrm{m}^2$, clamped on the left side along the contours $\Gamma_{D_1} = 0 \times (0, 0.1)$ and $\Gamma_{D_2} = 0 \times (0.9, 1.0)$, with a concentrated mass $m = 0.4$ located at the point $(3, 0.5)$, as depicted in Figure 1a. Figure 1b shows the displacement in the initial domain.

In Case B, the hold-all domain $\mathcal{D}$ is a rectangle $(0,6) \times (0,1), \mathrm{m}^2$, clamped at the point $(0,0)$ and simply supported at the point $(6,0)$. The concentrated masses $m = 0.7$ are located at the points $(1,1)$ and $(5,1)$, and an additional concentrated mass $m_1 = 1.4$ is located at the coordinate $(3,1)$, as depicted in Figure 2a. The displacement is shown in Figure 2b.

In Case C, the hold-all domain $\mathcal{D}$ is a rectangle $(0,4) \times (0,1), \mathrm{m}^2$. Concentrated masses $m = m_i$, where $i = 1, 2, \ldots, 11$ with $\sum m_i = 70$, are uniformly distributed along the upper side of the rectangle (see Figure 3a). Figure 3b shows the displacement in the initial domain.

Linear triangular finite elements were employed for discretization in all the cases presented.

Young's modulus is set as $E = 210$ GPa and contrast parameters as $\gamma_\alpha = \gamma_\rho = 10^{-3}$. Information on the initial grid, number of elements and number of nodes in the initial mesh, Poisson's ratio ν, and penalty parameter μ are expressed in Table 4, for each case.

Table 4. Considered cases.

Cases	Grid	Elements	Nodes	ν	μ
A	30 × 90	10,800	5521	0.25	1.4
B	30 × 180	21,600	11,011	0.3	0.7
C	10 × 40	1600	851	0.3	1.5

It should be noted that mesh refinement procedures were employed as part of the optimization scheme to improve the boundary resolution of the final topology. Table 4 provides details on the final mesh resulting from the refinement process.

To enhance accuracy and achieve smoother topologies, four levels of uniform mesh refinement were implemented during the iterative process for Cases A and B, and five levels for Case C.

The mesh refinement levels resulted in 2,764,600 elements and 1,384,321 nodes for Case A, 5,529,600 elements and 2,768,161 nodes for Case B, and 409,600 elements and 205,601 nodes for Case C.

The optimal topologies for Cases A, B, and C are illustrated in Figures 4–7, respectively. The effect of mesh refinement on the optimized topology for Case A is evident (see Figure 5). The final topology for Case B (Figure 6) exhibited asymmetry due to the boundary conditions, which included clamping at point (0,0) and simple support at point (6,0). In this example, the initial mesh comprises 19,200 elements (40 × 120 grid) and 9761 nodes, with all other parameters and boundary conditions consistent with those described for Case A.

Figure 8 introduces the normalized first eigenvalue history λ_1/λ_1^0 as the iterative process has evolved while Figure 9 depicts the normalized first eigenvalues' history λ_1/λ_2.

It can be observed that Case C achieved a higher ratio of λ_1/λ_2 compared to Cases A and B.

However, during the optimization process, no coincident eigenvalues were observed. Figures 10 and 11 illustrate the evolution of the shape functional and volume, respectively.

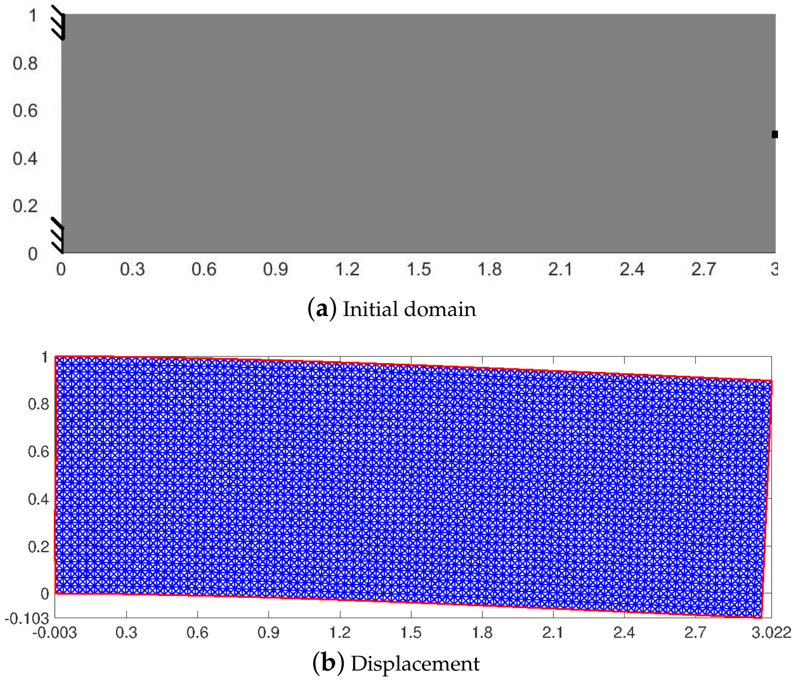

Figure 1. Case A: initial domain (**a**) and displacement (**b**).

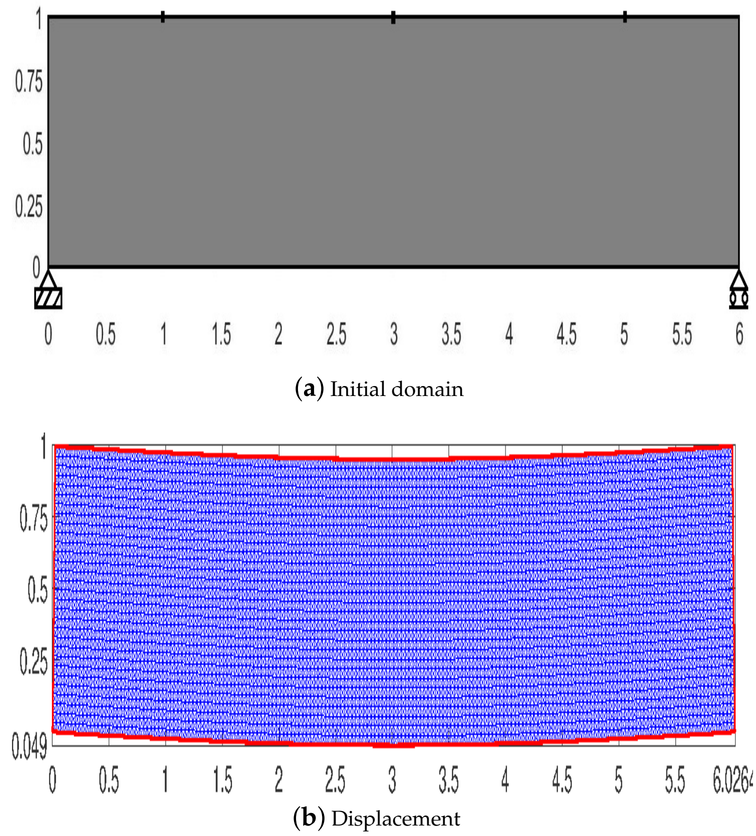

Figure 2. Case B: initial domain (**a**) and displacement (**b**).

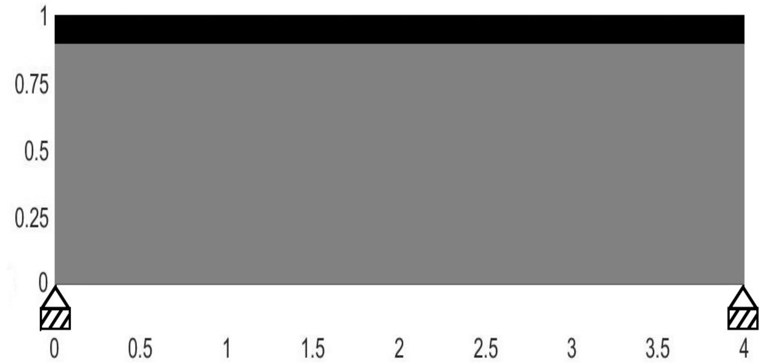

(**a**) Initial domain

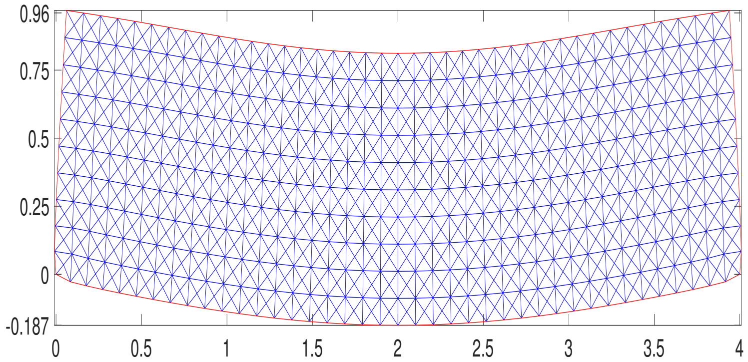

(**b**) Displacement

Figure 3. Case C: initial domain (**a**) and displacement (**b**).

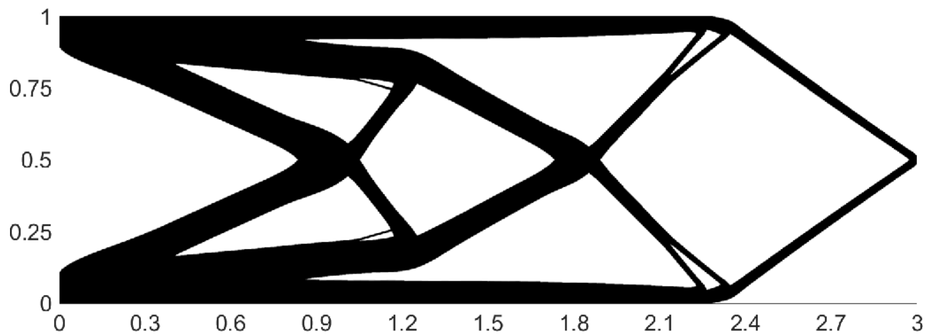

Figure 4. Optimized topology for Case A.

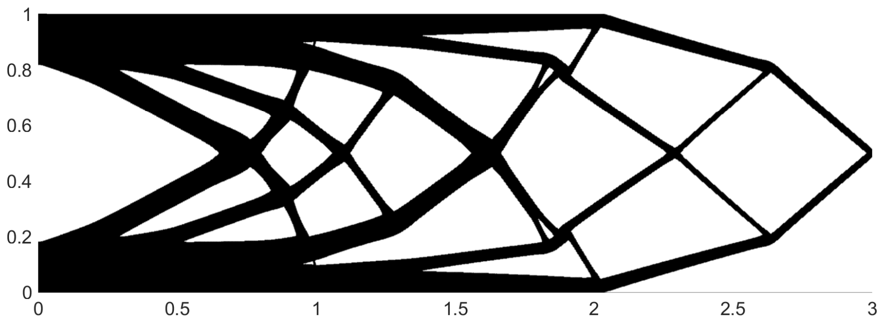

Figure 5. Optimized topology.

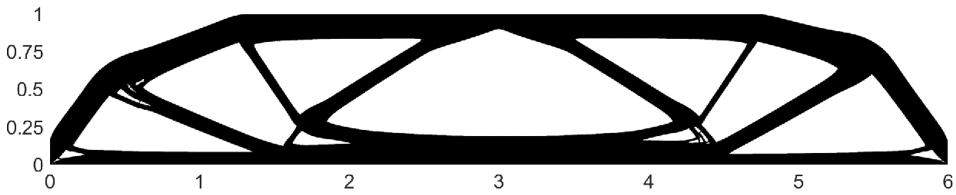

Figure 6. Optimized topology for Case B.

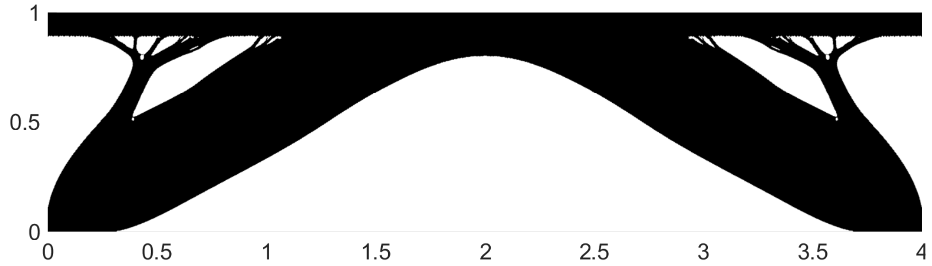

Figure 7. Optimized topology for Case C.

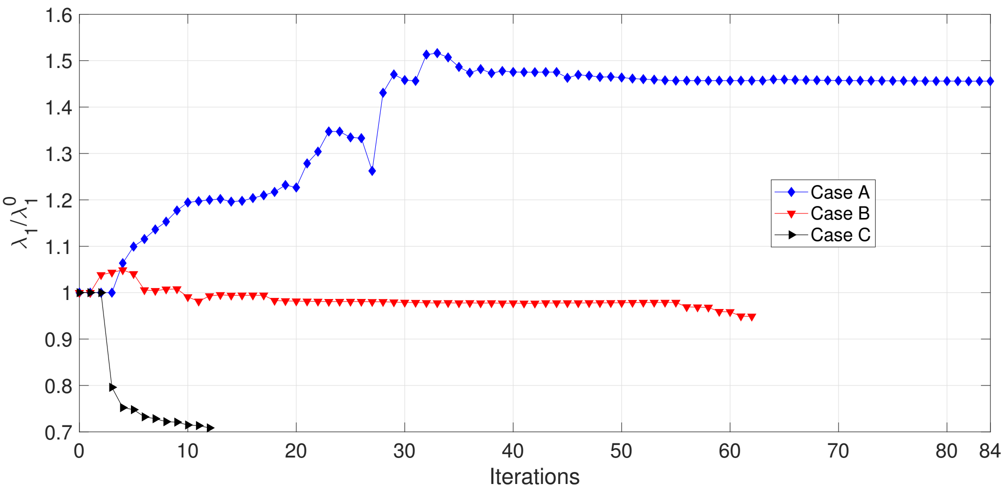

Figure 8. Normalized first eigenvalue λ_1/λ_1^0 history.

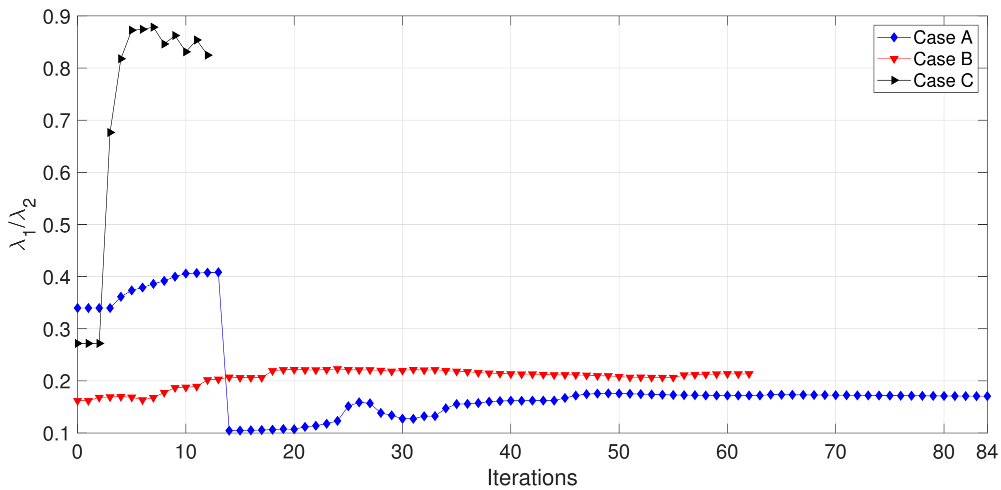

Figure 9. Normalized second eigenvalue λ_1/λ_2 history.

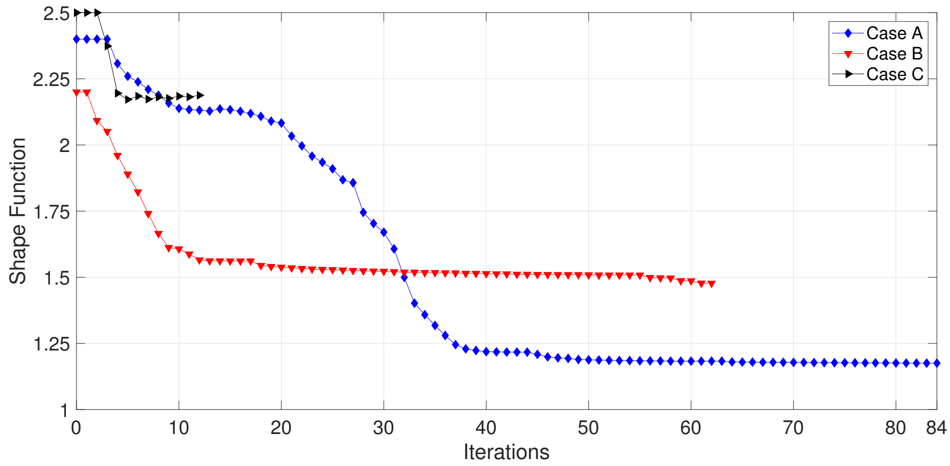

Figure 10. Shape function history.

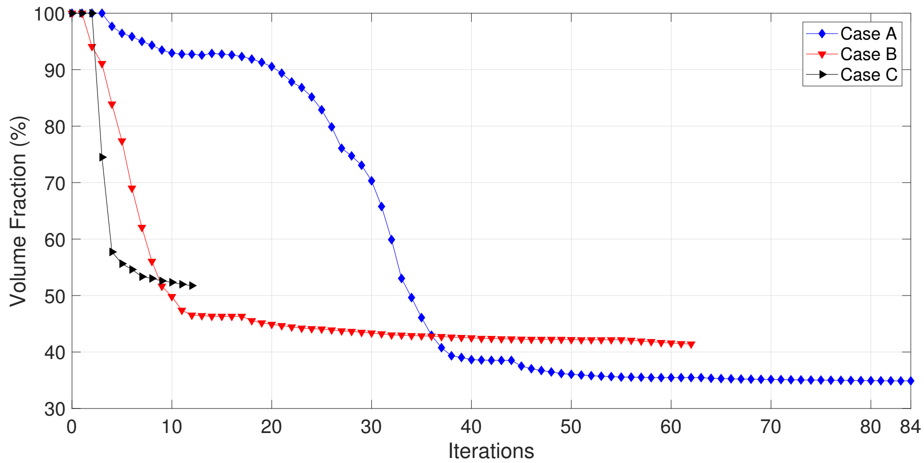

Figure 11. Volume fraction history.

To evaluate the influence of the parameter μ on the final design, a set of four cases is considered. Variations in the parameter μ are detailed in Table 5.

Table 5. Penalty parameter.

	Case D1	**Case D2**	**Case D3**	**Case D4**
μ	0.5	1.0	1.5	2.0

For Cases D1, D2, D3, and D4, the hold-all domain $\mathcal{D}$ is a unit square $(0,1) \times (0,1)$, m^2, clamped at the points $(0,0)$ and $(0,1)$. A concentrated mass $m = 0.1$ is applied at the point $(1,1)$, as shown in Figure 12a, with the initial displacement depicted in Figure 12b.

The final topologies for each case are presented in Figure 13a–d. Figures 14 and 15 show the history of the shape functional and volume fraction, respectively.

The history of the normalized first eigenvalue, λ_1/λ_1^0 (where λ_1^0 is its initial value), is illustrated in Figure 16, showing the evolution until the process is halted.

Figure 17 depicts the history of the normalized first eigenvalue ratio, λ_1/λ_2. As before, no presence of multiple eigenvalues was observed.

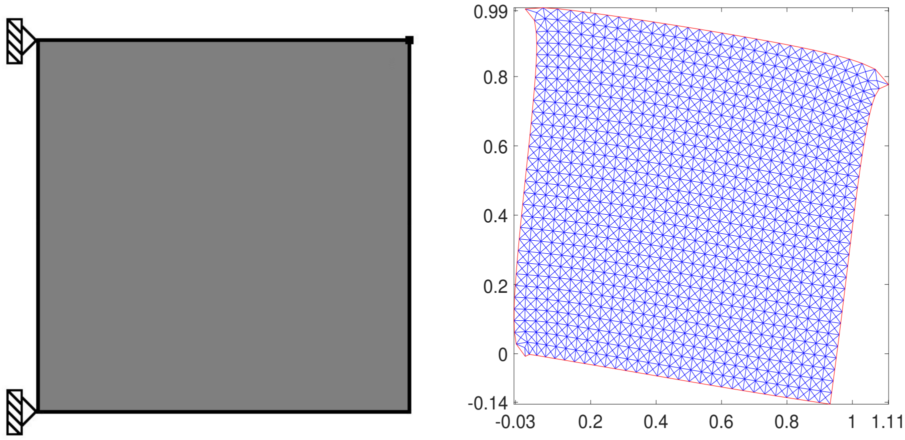

(**a**) Inital domain (**b**) Displacement

Figure 12. Cases D1, D2, D3, and D4: initial domain (**a**) and displacement (**b**).

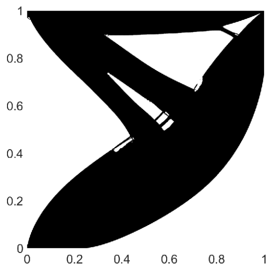

(**a**) Case D1

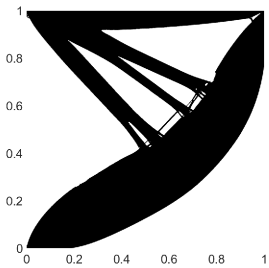

(**b**) Case D2

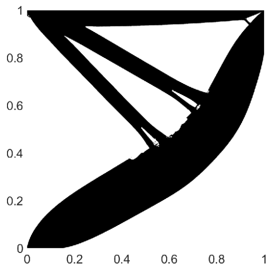

(**c**) Case D3

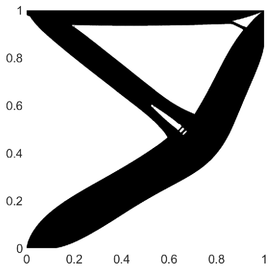

(**d**) Case D4

Figure 13. Comparison of designs obtained for Cases D1, D2, D3, and D4.

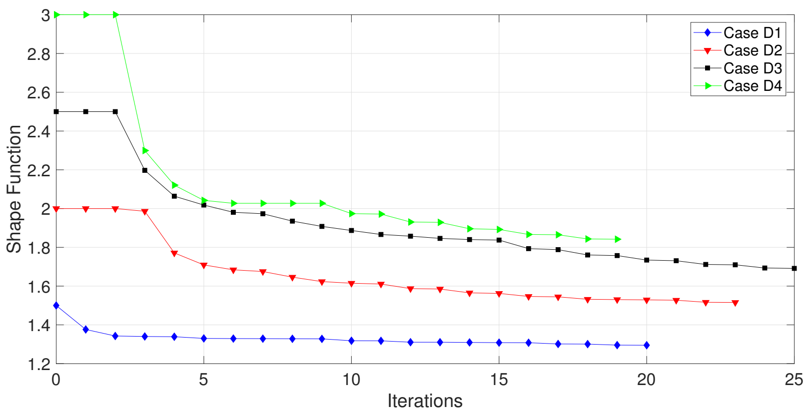

Figure 14. Cases D1, D2, D3, and D4: shape function history.

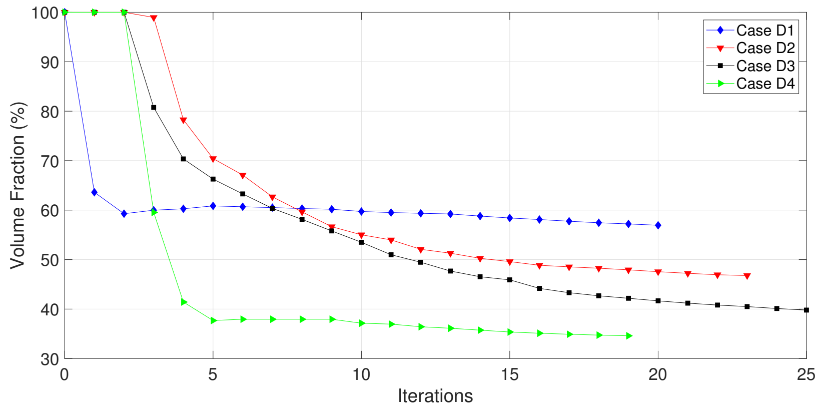

Figure 15. Cases D1, D2, D3, and D4: volume fraction history.

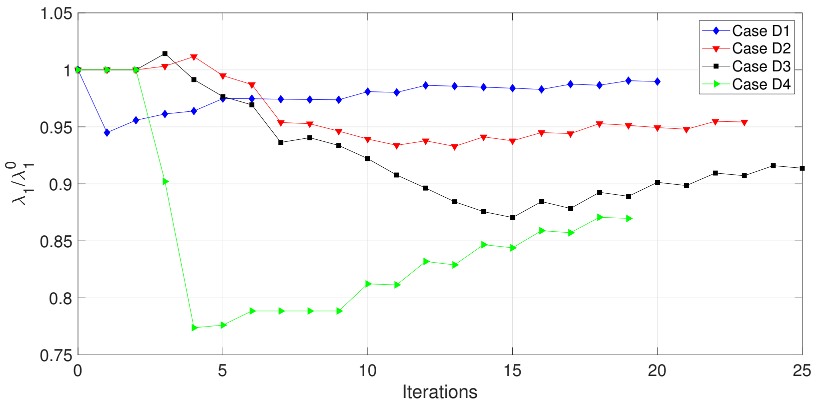

Figure 16. Cases D1, D2, D3, and D4: normalized first eigenvalue λ_1/λ_1^0 history.

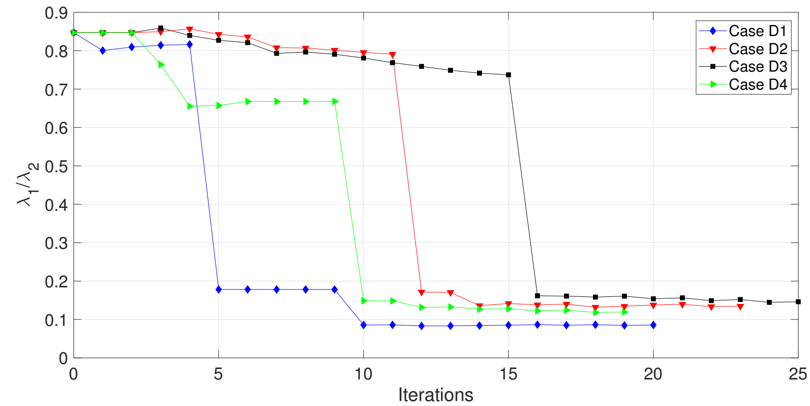

Figure 17. Cases D1, D2, D3, and D4: normalized second eigenvalue λ_1/λ_2 history.

4. Conclusions

In this work, the associated topological derivative of the first eigenvalue for plane structure problems was used for topology optimization. The convergence to a local minimum was achieved by combining the level set method with the analytical formula for the topological derivative (D_T). While coincident eigenvalues are often encountered in this type of problem, they were not observed in the present work. The algorithm converged successfully for all numerical examples, and no special methods were needed to handle multiple eigenvalues. The results highlight the effectiveness of the D_T concept in deriving optimal topologies for eigenvalue problems in plane structures.

Author Contributions: Writing—original draft, F.S.C. and C.T.M.A. All authors have read and agreed to the published version of the manuscript.

Funding: This research received no external funding.

Data Availability Statement: Some or all data or code generated or used during the study are available from the corresponding author by reasonable request (ETABS command lines files and MATLAB R2022a code used to perform analyses).

Acknowledgments: The authors gratefully acknowledge the valuable contributions given by A.A. Novotny during the topological derivative mathematical development. Additionally, the authors also extend their thanks to S.M. Giusti for kindly sharing the numerical routine, which was adapted for the present topology optimization procedure. Finally, we would like to express our gratitude to Dirley Rucheinsky (in memoriam) for his valuable contributions to the numerical results presented in this work.

Conflicts of Interest: No potential conflicts of interest were reported by the authors.

Appendix A. Topological Asymptotic Analysis

Let us introduce an ansatz for the solution u_ε to the perturbed boundary value problem (7) of the form

$$u_\varepsilon(x) = u(x) + w_\varepsilon(x) + \widetilde{u}_\varepsilon(x), \tag{A1}$$

where u is the solution to the unperturbed boundary value problem (2), w_ε is the solution to an exterior boundary value problem, and $\widetilde{u}_\varepsilon$ is the remainder.

In particular, the exterior problem reads as follows: Find w_ε, such that

$$\left\{ \begin{array}{rcll} \operatorname{div}(\alpha_\varepsilon \sigma(w_\varepsilon)) & = & 0 & \text{in} \quad R^2\,, \\ w_\varepsilon & \to & 0 & \text{at} \quad \infty \\ \left.\begin{array}{r} (w_\varepsilon) \\ (\alpha_\varepsilon \sigma(w_\varepsilon)) \cdot n \end{array}\right. & \begin{array}{c} = \\ = \end{array} & \left.\begin{array}{c} 0 \\ g \end{array}\right\} & \text{on} \quad \partial B_\varepsilon\,, \end{array} \right. \tag{A2}$$

where $g = (1 - \gamma_\alpha)\alpha\sigma u(\widehat{x}) \cdot n$. The above boundary value problem admits an explicit solution (see, for instance, the book by Novotny and Sokolowski [16]), which can be written in a polar coordinate system (r, θ) with a center at $\widehat{x}$, as follows:

For $r \geq \varepsilon$ (outside the inclusion),

$$\sigma^{rr}(w_\varepsilon(r,\theta)) = -\varphi_1\left(\frac{1-\gamma_\alpha}{1+\gamma_\alpha a_1}\frac{\varepsilon^2}{r^2}\right) - \varphi_2\left(4\frac{1-\gamma_\alpha}{1+\gamma_\alpha a_2}\frac{\varepsilon^2}{r^2} + 3\frac{1-\gamma_\alpha}{1+\gamma_\alpha a_2}\frac{\varepsilon^4}{r^4}\right) cos\,2\theta, \tag{A3}$$

$$\sigma^{\theta\theta}(w_\varepsilon(r,\theta)) = -\varphi_1\left(\frac{1-\gamma_\alpha}{1+\gamma_\alpha a_1}\frac{\varepsilon^2}{r^2}\right) - \varphi_2\left(3\frac{1-\gamma_\alpha}{1+\gamma_\alpha a_2}\frac{\varepsilon^4}{r^4}\right) cos\,2\theta, \tag{A4}$$

$$\sigma^{r\theta} = -\varphi_2\left(2\frac{1-\gamma_\alpha}{1+\gamma_\alpha a_2}\frac{\varepsilon^2}{r^2} - 3\frac{1-\gamma_\alpha}{1+\gamma_\alpha a_2}\frac{\varepsilon^4}{r^4}\right) sin\,2\theta. \tag{A5}$$

For $0 < r < \varepsilon$ (inside the inclusion),

$$\sigma^{rr}(w_\varepsilon(r,\theta)) = \varphi_1\left(a_1\gamma_\alpha\frac{1-\gamma_\alpha}{1+\gamma_\alpha a_1}\right) + \varphi_2\left(a_2\gamma_\alpha\frac{1-\gamma_\alpha}{1+\gamma_\alpha a_2}\right) cos\,2\theta, \tag{A6}$$

$$\sigma^{\theta\theta}(w_\varepsilon(r,\theta)) = \varphi_1\left(a_1\gamma_\alpha\frac{1-\gamma_\alpha}{1+\gamma_\alpha a_1}\right) - \varphi_2\left(a_2\gamma_\alpha\frac{1-\gamma_\alpha}{1+\gamma_\alpha a_2}\right) cos\,2\theta, \tag{A7}$$

$$\sigma^{r\theta}(w_\varepsilon(r,\theta)) = -\varphi_2\left(a_2\gamma_\alpha\frac{1-\gamma_\alpha}{1+\gamma_\alpha a_2}\right) sin\,2\theta. \tag{A8}$$

Some terms in the above formulae require explanations. The coefficients φ_1 and φ_2 are given by

$$\varphi_1 = \frac{1}{2}(\sigma_1(u(\widehat{x})) + \sigma_2(u(\widehat{x}))), \qquad \varphi_1 = \frac{1}{2}(\sigma_1(u(\widehat{x})) - \sigma_2(u(\widehat{x}))), \tag{A9}$$

where $\sigma_1(u(\widehat{x}))$ and $\sigma_2(u(\widehat{x}))$ are the eigenvalues of tensor $\sigma(u(\widehat{x}))$, which can be expressed as

$$\sigma_{1,2}(u(\widehat{x})) = \frac{1}{2}\left(tr\,\sigma(u(\widehat{x})) \pm \sqrt{2\sigma^D(u(\widehat{x}))\cdot\sigma^D(u(\widehat{x}))}\right), \quad \text{(A10)}$$

with $\sigma^D(u(\widehat{x}))$ standing for the deviatory part of the stress tensor $\sigma(u(\widehat{x}))$, namely,

$$\sigma^D(u(\widehat{x})) = \sigma(u(\widehat{x})) - \frac{1}{2}tr\,\sigma(u(\widehat{x}))\mathbf{I}. \quad \text{(A11)}$$

In addition, the constants a_1 and a_2 are given by

$$a_1 = \frac{\mu+\lambda}{\mu}, \qquad \frac{3\mu+\lambda}{\mu+\lambda}. \quad \text{(A12)}$$

Finally, $\sigma^{rr}(u_\varepsilon)$, $\sigma^{\theta\theta}(u_\varepsilon)$, and $\sigma^{r\theta}(u_\varepsilon)$ are the components of tensor $\sigma(u_\varepsilon)$ in the polar coordinate system, namely, $\sigma^{rr}(u_\varepsilon) = e^r\cdot\sigma(u_\varepsilon)e^r$, $\sigma^{\theta\theta}(u_\varepsilon) = e^\theta\cdot\sigma(u_\varepsilon)e^\theta$, and $\sigma^{r\theta}(u_\varepsilon) = e^r\cdot\sigma(u_\varepsilon)e^\theta$, with e^r and e^θ used to denote the canonical basis associated with the polar coordinate system (r,θ)), such that $\|e^r\| = \|e^\theta\| = 1$ and $e^r\cdot e^\theta = 0$ (for more details, see [16]).

Note that the remainder is constructed in order to compensate for the discrepancies introduced by the boundary layers w_ε and by the higher-order terms of the Taylor series expansion of $\sigma(u)$ around the point $\widehat{x}\in\Omega$. It means that $\widetilde{u}_\varepsilon$ has to be the solution to the following boundary value problem: Find $\widetilde{u}_\varepsilon$, such that

$$\left\{\begin{array}{rcll} -\text{div}[\alpha_\varepsilon\sigma(\widetilde{u}_\varepsilon)(x)] + \rho_\varepsilon k\widetilde{u}_\varepsilon(x) &=& \rho_\varepsilon k w_\varepsilon & \text{in} \quad \Omega, \\ \widetilde{u}_\varepsilon &=& \varepsilon^2 g_1 & \text{on} \quad \partial\Omega, \\ (\widetilde{u}_\varepsilon) &=& 0 & \multirow{2}{*}{on ∂B_ε ,} \\ (\alpha_\varepsilon\sigma(\widetilde{u}_\varepsilon))n &=& \varepsilon g_2 & \end{array}\right. \quad \text{(A13)}$$

with functions $g_1 = -\varepsilon^{-2}w_\varepsilon$ and $g_2 = (1-\gamma_\alpha)\alpha[\sigma(w_\varepsilon]n\cdot n$ independent of ε.

Lemma A1. *Let $\widetilde{u}_\varepsilon$ be the solution of (A13) or, equivalently, of the following variational problem*

$$\widetilde{u}_\varepsilon \in \widetilde{\mathcal{U}}_\varepsilon : \int_\Omega \alpha_\varepsilon\sigma(\widetilde{u}_\varepsilon)\cdot\nabla v + \int_\Omega \rho_\varepsilon k\widetilde{u}_\varepsilon v + = \int_\Omega \rho_\varepsilon k w_\varepsilon v + \varepsilon\int_{\partial B_\varepsilon} g_2 v, \quad \forall v\in H_0^1(\Omega), \quad \text{(A14)}$$

where the set $\widetilde{\mathcal{U}}_\varepsilon := \{\varphi\in H^1(\Omega) : \varphi_{|\partial\Omega} = \varepsilon^2 g_1\}$. Then, the estimate $\|\widetilde{u}_\varepsilon\|_{H^1(\Omega)} = o(\varepsilon)$ holds true.

By setting $v = \widetilde{u}_\varepsilon - \varphi_\varepsilon \in H_0^1(\Omega)$ as the test function in (A14), where $\varphi_\varepsilon\in\widetilde{\mathcal{U}}_\varepsilon$ is the lifting of the Dirichlet data $\varepsilon^2 g_1$ on $\partial\Omega$, we have

$$\int_\Omega \alpha_\varepsilon\sigma(\widetilde{u}_\varepsilon)\cdot\nabla^s\widetilde{u}_\varepsilon + \int_\Omega \rho_\varepsilon k|\widetilde{u}_\varepsilon|^2 = \underbrace{\varepsilon^2\int_{\partial\Omega} g_1\alpha\partial_n\widetilde{u}_\varepsilon}_{E_1} + \underbrace{\varepsilon\int_{\partial B_\varepsilon} g_2\widetilde{u}_\varepsilon}_{E_2} - \underbrace{\int_\Omega \rho_\varepsilon k w_\varepsilon\widetilde{u}_\varepsilon}_{E_3}. \quad \text{(A15)}$$

Therefore, from the Cauchy–Schwarz inequality, there are

$$|E_1| = \varepsilon^2\left|\int_{\partial\Omega} g_1\alpha\partial_n\widetilde{u}_\varepsilon\right| \leqslant \varepsilon^2\|g_1\|_{L^2(\partial\Omega)}\|\partial_n\widetilde{u}_\varepsilon\|_{L^2(\partial\Omega)} \leqslant C_1\varepsilon^2\|\widetilde{u}_\varepsilon\|_{H^1(\Omega)}, \quad \text{(A16)}$$

$$|E_2| = \varepsilon\left|\int_{\partial B_\varepsilon} g_2\widetilde{u}_\varepsilon\right| \leqslant \varepsilon\|g_2\|_{L^2(\partial B_\varepsilon)}\|\widetilde{u}_\varepsilon\|_{L^2(\partial B_\varepsilon)} \leqslant C_2\varepsilon^{3/2}\|\widetilde{u}_\varepsilon\|_{H^1(\Omega)}, \quad \text{(A17)}$$

$$|E_3| = \left|\int_\Omega \rho_\varepsilon k w_\varepsilon\widetilde{u}_\varepsilon\right| \leqslant \|w_\varepsilon\|_{L^2(\Omega)}\|\widetilde{u}_\varepsilon\|_{L^2(\Omega)} \leqslant C_3\varepsilon^2\sqrt{|\ln(\varepsilon)|}\|\widetilde{u}_\varepsilon\|_{H^1(\Omega)}. \quad \text{(A18)}$$

From these last results, we obtain

$$\int_\Omega \rho_\varepsilon \sigma(\widetilde{u}_\varepsilon) \cdot \nabla^s \widetilde{u}_\varepsilon + \int_\Omega \rho_\varepsilon k |\widetilde{u}_\varepsilon|^2 \leqslant C_5(\varepsilon^2 + \varepsilon^{3/2} + \varepsilon^2 \sqrt{|\ln(\varepsilon)|}) \|\widetilde{u}_\varepsilon\|_{H^1(\Omega)}. \tag{A19}$$

By taking into account the coercivity of the bilinear form on the left-hand side of the above inequality, there is

$$c\|\widetilde{u}_\varepsilon\|^2_{H^1(\Omega)} \leqslant \int_\Omega \rho_\varepsilon \sigma(\widetilde{u}_\varepsilon) \cdot \nabla^s \widetilde{u}_\varepsilon + \int_\Omega \rho_\varepsilon k |\widetilde{u}_\varepsilon|^2, \tag{A20}$$

which leads to the result with constants c and C_5 independent of ε.

Corollary A1. *Let u and u_ε be solutions of problems (2) and (7), respectively. Then,*

$$\|u_\varepsilon - u\|_{L^2(\Omega)} = o(\varepsilon). \tag{A21}$$

By taking into account the ansatz (A1) and the triangular inequality, it follows that

$$\begin{aligned} \|u_\varepsilon - u\|_{L^2(\Omega)} &= \|w_\varepsilon + \widetilde{u}_\varepsilon\|_{L^2(\Omega)} \\ &\leqslant \|w_\varepsilon\|_{L^2(\Omega)} + \|\widetilde{u}_\varepsilon\|_{L^2(\Omega)} \\ &\leqslant \|w_\varepsilon\|_{L^2(\Omega)} + \|\widetilde{u}_\varepsilon\|_{H^1(\Omega)} = o(\varepsilon). \end{aligned} \tag{A22}$$

where we have used Lemma A1.

Before proceeding, let us subtract (2) from (7). After a simple manipulation by taking into account the contrasts (Tables 2 and 3), one can obtain

$$\begin{aligned} \int_\Omega \alpha\sigma(u_\varepsilon - u) \cdot \nabla^s v + \int_\Omega \rho k (u_\varepsilon - u) v = \int_{B_\varepsilon} (1-\gamma_\alpha)\alpha\sigma(u_\varepsilon) \cdot \nabla^s v + \\ \int_{B_\varepsilon} (1-\gamma_\rho)\rho k u_\varepsilon v - \int_{B_\varepsilon} (1-\gamma_\beta)\beta f v. \end{aligned} \tag{A23}$$

Appendix A.1. Proof of Theorem 1

By subtracting $\mathcal{G}(u)$ from $\mathcal{G}_\varepsilon(u_\varepsilon)$, there is

$$\mathcal{G}_\varepsilon(u_\varepsilon) - \mathcal{G}(u) = \underbrace{2\int_\Omega \rho k (u_\varepsilon - u) u}_{A_1} - \underbrace{\int_{B_\varepsilon} (1-\gamma_\rho)\rho k |u_\varepsilon|^2}_{A_2} + \underbrace{\int_\Omega \rho k |u_\varepsilon - u|^2}_{\mathcal{E}_1(\varepsilon)}, \tag{A24}$$

with the remainder $\mathcal{E}_1(\varepsilon)$ bounded as follows:

$$|\mathcal{E}_1(\varepsilon)| \leqslant C_1 \|u_\varepsilon - u\|^2_{L^2(\Omega)} = o(\varepsilon^2), \tag{A25}$$

where we have used Corollary A1. The integral A_2 can be trivially expanded as follows:

$$\begin{aligned} A_2 = \pi\varepsilon^2(1-\gamma_\rho)\rho k |u|^2(\widehat{x}) + \underbrace{\int_{B_\varepsilon} (1-\gamma_\rho)\rho k |u_\varepsilon - u|^2}_{\mathcal{E}_2(\varepsilon)} \\ + \underbrace{2\int_{B_\varepsilon} (1-\gamma_\rho)\rho k (u_\varepsilon - u) u}_{\mathcal{E}_3(\varepsilon)} + \underbrace{\int_{B_\varepsilon} (1-\gamma_\rho)\rho k [|u|^2 - |u(\widehat{x})|^2]}_{\mathcal{E}_4(\varepsilon)}. \end{aligned} \tag{A26}$$

with remainders $\mathcal{E}_2(\varepsilon)$, $\mathcal{E}_3(\varepsilon)$, and $\mathcal{E}_4(\varepsilon)$ bounded as follows:

$$|\mathcal{E}_2(\varepsilon)| \leqslant C_2\|u_\varepsilon - u\|^2_{L^2(\Omega)} = o(\varepsilon^2), \quad (A27)$$
$$|\mathcal{E}_3(\varepsilon)| \leqslant C_3\varepsilon\|u_\varepsilon - u\|_{L^2(\Omega)} = o(\varepsilon^2), \quad (A28)$$
$$|\mathcal{E}_4(\varepsilon)| \leqslant C_4\|x - \widehat{x}\|^2_{L^2(B_\varepsilon)} = o(\varepsilon^2). \quad (A29)$$

where we have used Corollary A1 together with the interior elliptic regularity of function u. Now, let us set $v = q$ in (A23) and $v = u_\varepsilon - u$ in the adjoint Equation (5). After comparing the obtained results, the integral A_1 can be rewritten as

$$A_1 = -\underbrace{\int_{B_\varepsilon}(1-\gamma_\alpha)\alpha\sigma(u_\varepsilon)\cdot\nabla^s q}_{A_3} - \underbrace{\int_{B_\varepsilon}(1-\gamma_\rho)\rho k u_\varepsilon q}_{A_4} + \underbrace{\int_{B_\varepsilon}(1-\gamma_\beta)\beta f q}_{A_5}. \quad (A30)$$

The integrals A_5 and A_6 are trivially expanded as

$$A_4 = \pi\varepsilon^2(1-\gamma_\rho)\rho k u q(\widehat{x}) + \underbrace{\int_{B_\varepsilon}(1-\gamma_\rho)\rho k(u_\varepsilon - u)q}_{\mathcal{E}_5(\varepsilon)} + \underbrace{\int_{B_\varepsilon}(1-\gamma_\rho)\rho k[uq - uq(\widehat{x})]}_{\mathcal{E}_6(\varepsilon)}, \quad (A31)$$
$$A_5 = \pi\varepsilon^2(1-\gamma_\beta)\beta f q(\widehat{x}) + \underbrace{\int_{B_\varepsilon}(1-\gamma_\beta)\beta f[q - q(\widehat{x})]}_{\mathcal{E}_7(\varepsilon)}. \quad (A32)$$

with the remainders $\mathcal{E}_5(\varepsilon)$, $\mathcal{E}_6(\varepsilon)$, and $\mathcal{E}_7(\varepsilon)$ bounded as follows:

$$|\mathcal{E}_5(\varepsilon)| \leqslant \varepsilon\|u_\varepsilon - u\|_{L^2(\Omega)} = o(\varepsilon^2), \quad (A33)$$
$$|\mathcal{E}_6(\varepsilon)| \leqslant \varepsilon\|x - \widehat{x}\|_{L^2(B_\varepsilon)} = o(\varepsilon^2), \quad (A34)$$
$$|\mathcal{E}_7(\varepsilon)| \leqslant \varepsilon\|x - \widehat{x}\|_{L^2(B_\varepsilon)} = o(\varepsilon^2), \quad (A35)$$

where we have used Corollary A1 and the interior elliptic regularity of functions u and q. The integrals A_3 and A_4 can be developed in the following way,

$$A_3 + A_4 = \underbrace{\int_{B_\varepsilon}(1-\gamma_\alpha)\alpha\sigma(u)\cdot\nabla^s q}_{A_6} + \underbrace{\int_{B_\varepsilon}(1-\gamma_\alpha)\alpha\sigma(w_\varepsilon)\cdot\nabla^s q}_{A_7} + \underbrace{\int_{B_\varepsilon}(1-\gamma_\alpha)\alpha\sigma(\tilde{u}_\varepsilon)\cdot\nabla^s q}_{\mathcal{E}_8(\varepsilon)}, \quad (A36)$$

where we have introduced the ansatz (A1). Therefore,

$$A_6 = \pi\varepsilon^2(1-\gamma_\alpha)\alpha\sigma(u)\cdot\nabla^s q(\widehat{x}) + \underbrace{\int_{B_\varepsilon}(1-\gamma_\alpha)\alpha[\sigma(u)\cdot\nabla^s q - \sigma(u)\cdot\nabla^s q(\widehat{x})]}_{\mathcal{E}_9(\varepsilon)}, \quad (A37)$$

with remainders $\mathcal{E}_8(\varepsilon)$ and $\mathcal{E}_9(\varepsilon)$ bounded as follows:

$$|\mathcal{E}_8(\varepsilon)| \leqslant \varepsilon\|\tilde{u}_\varepsilon\|_{H^1(\Omega)} = o(\varepsilon^2), \quad (A38)$$
$$|\mathcal{E}_9(\varepsilon)| \leqslant \varepsilon\|\tilde{u}_\varepsilon\|_{H^1(\Omega)} = o(\varepsilon^2). \quad (A39)$$

where we have used Lemma A1 together with the interior elliptic regularity of functions u and q. The last two integral A_7 can be rewritten as

$$A_7 = \pi\varepsilon^2(1-\gamma_\alpha)\alpha\mathbb{P}\sigma(u)\cdot\nabla^s q(\widehat{x}) + \underbrace{\int_{B_\varepsilon}(1-\gamma_\alpha)\alpha\sigma(w_\varepsilon)\cdot\nabla^s(q-q(\widehat{x}))}_{\mathcal{E}_{10}(\varepsilon)}, \quad \text{(A40)}$$

where we have used the explicit solution (A6)–(A8). The remainder $\mathcal{E}_{10}(\varepsilon)$ can be bounded as follows:

$$|\mathcal{E}_{10}(\varepsilon)| \leqslant C_5\|\nabla^s w_\varepsilon\|_{L^2(B_\varepsilon)}\|x-\widehat{x}\|_{L^2(B_\varepsilon)} = o(\varepsilon^2). \quad \text{(A41)}$$

Finally, after collecting the obtained results, we have

$$\mathcal{G}_\varepsilon(u_\varepsilon) - \mathcal{G}(u) = -\pi\varepsilon^2[2\alpha\mathbb{P}\sigma(u)\cdot\nabla^s q(\widehat{x}) + (1-\gamma_\rho)\rho k u(u+q)(\widehat{x}) - (1-\gamma_\beta)\beta f q(\widehat{x})] + \sum_{i=1}^{10}\mathcal{E}_i(\varepsilon), \quad \text{(A42)}$$

where the remainders $\mathcal{E}_i(\varepsilon) = o(\varepsilon^2)$ for $i = 1\cdots 10$. □

Appendix A.2. Proof of Theorem 2

Let us subtract $\mathcal{J}(u)$ from $\mathcal{J}_\varepsilon(u_\varepsilon)$ to obtain

$$\mathcal{J}_\varepsilon(u_\varepsilon) - \mathcal{J}(u) = 2\int_\Omega \alpha\sigma(u_\varepsilon - u)\cdot\nabla^s u - \int_{B_\varepsilon}(1-\gamma_\alpha)\alpha\sigma(u_\varepsilon)\cdot\nabla^s u_\varepsilon + \underbrace{\int_\Omega \alpha\sigma(u_\varepsilon-u)\cdot\nabla^s(u_\varepsilon-u)}_{B_1}. \quad \text{(A43)}$$

By setting $v = u_\varepsilon - u$ as the test function in (A23), the integral B_1 can be rewritten, after some manipulations, as

$$B_1 = \int_{B_\varepsilon}(1-\gamma_\alpha)\alpha\sigma(u_\varepsilon)\cdot\nabla^s(u_\varepsilon-u) + \mathcal{E}_{11}(\varepsilon). \quad \text{(A44)}$$

The remainder $\mathcal{E}_{11}(\varepsilon)$ is defined as

$$\mathcal{E}_{11}(\varepsilon) = \int_{B_\varepsilon}(1-\gamma_\rho)\rho k|u_\varepsilon-u|^2 + \int_{B_\varepsilon}(1-\gamma_\rho)\rho k u(u_\varepsilon-u) - \int_{B_\varepsilon}(1-\gamma_\beta)\beta f(u_\varepsilon-u) - \int_\Omega \rho k|u_\varepsilon-u|^2, \quad \text{(A45)}$$

which can be bounded as follows:

$$\begin{aligned} |\mathcal{E}_{11}(\varepsilon)| &\leqslant C_1(\varepsilon + \|u_\varepsilon-u\|_{L^2(B_\varepsilon)} + \|\nabla^s(u_\varepsilon-u)\|_{L^2(B_\varepsilon)})\|u_\varepsilon-u\|_{L^2(B_\varepsilon)} \\ &+ C_2(\|u_\varepsilon-u\|_{L^2(\Omega)} + \|\nabla^s(u_\varepsilon-u)\|_{L^2(\Omega)})\|u_\varepsilon-u\|_{L^2(\Omega)} \\ &\leqslant C_3\|u_\varepsilon-u\|_{L^2(\Omega)}\|u_\varepsilon-u\|_{H^1(\Omega)} = o(\varepsilon^2), \end{aligned} \quad \text{(A46)}$$

where we have used the Cauchy–Schwarz inequality together with Lemma 1 and Corollary A1. Therefore, equation (A43) becomes

$$\mathcal{J}_\varepsilon(u_\varepsilon) - \mathcal{J}(u) = \underbrace{2\int_\Omega \alpha\sigma(u_\varepsilon-u)\cdot\nabla^s u}_{B_2} - \underbrace{\int_{B_\varepsilon}(1-\gamma_\alpha)\alpha\sigma(u_\varepsilon)\cdot\nabla^s u}_{B_3} + \mathcal{E}_{11}(\varepsilon). \quad \text{(A47)}$$

From the ansatz (A1), integral B_3 can be written as

$$B_3 = \underbrace{\int_{B_\varepsilon} (1-\gamma_\alpha)\alpha\sigma(u)\cdot\nabla^s u}_{B_4} + \underbrace{\int_{B_\varepsilon} (1-\gamma_\alpha)\alpha\sigma(w_\varepsilon)\cdot\nabla^s u}_{B_5} + \underbrace{\int_{B_\varepsilon} (1-\gamma_\alpha)\alpha\sigma(u)\cdot\nabla^s \widetilde{u}_\varepsilon}_{\mathcal{E}_{12}(\varepsilon)}, \tag{A48}$$

with the remainder $\mathcal{E}_{12}(\varepsilon)$ bounded as follows:

$$|\mathcal{E}_{12}(\varepsilon)| \leqslant C_1\varepsilon\|\nabla^s\widetilde{u}_\varepsilon\|_{L^2(B_\varepsilon)} \leqslant C_2\varepsilon\|\widetilde{u}_\varepsilon\|_{H^1(\Omega)} = o(\varepsilon^2) \tag{A49}$$

where we have used Lemma A1. The integrals B_4 and B_5 can be trivially expanded as follows:

$$B_4 = \pi\varepsilon^2(1-\gamma_\alpha)\alpha\sigma(u(\widehat{x}))\cdot\nabla^s u(\widehat{x}) + \underbrace{\int_{B_\varepsilon}(1-\gamma_\alpha)\alpha(\sigma(u)\cdot\nabla^s u - \sigma(u(\widehat{x}))\cdot\nabla^s u(\widehat{x})}_{\mathcal{E}_{13}(\varepsilon)}, \tag{A50}$$

$$B_5 = \pi\varepsilon^2(1-\gamma_\alpha)\alpha\mathbb{P}\sigma(u)\cdot\nabla^s u(\widehat{x}) + \underbrace{\int_{B_\varepsilon}(1-\gamma_\alpha)\alpha\sigma(w_\varepsilon)\cdot(\nabla^s u - \nabla^s u(\widehat{x}))}_{\mathcal{E}_{14}(\varepsilon)}, \tag{A51}$$

where we have used the explicit solution (A6)–(A8). The remainders $\mathcal{E}_{13}(\varepsilon)$ and $\mathcal{E}_{14}(\varepsilon)$ can be bounded as follows:

$$|\mathcal{E}_{13}(\varepsilon)| \leqslant C_1\varepsilon\|x-\widehat{x}\|_{L^2(B_\varepsilon)} = o(\varepsilon^2), \tag{A52}$$

$$|\mathcal{E}_{14}(\varepsilon)| \leqslant C_2\|\sigma(w_\varepsilon)\|_{L^2(B_\varepsilon)}\|x-\widehat{x}\|_{L^2(B_\varepsilon)} = o(\varepsilon^2). \tag{A53}$$

Now, let us set $v = p$ in (A23) and $v = u_\varepsilon - u$ in the adjoint Equation (6). After comparing the obtained results, the integral B_2 can be rewritten as

$$B_2 = -\underbrace{\int_{B_\varepsilon}(1-\gamma_\alpha)\alpha\sigma(u_\varepsilon)\cdot\nabla^s p}_{B_6} - \underbrace{\int_{B_\varepsilon}(1-\gamma_\rho)\rho k u_\varepsilon p}_{B_7} + \underbrace{\int_{B_\varepsilon}(1-\gamma_\beta)\beta f p}_{B_8}. \tag{A54}$$

The integrals B_7 and B_8 are trivially expanded as

$$B_7 = \pi\varepsilon^2(1-\gamma_\rho)\rho k u p(\widehat{x}) + \underbrace{\int_{B_\varepsilon}(1-\gamma_\rho)\rho k(u_\varepsilon - u)p}_{\mathcal{E}_{15}(\varepsilon)} + \underbrace{\int_{B_\varepsilon}(1-\gamma_\rho)\rho k[up - up(\widehat{x})]}_{\mathcal{E}_{16}(\varepsilon)}, \tag{A55}$$

$$B_8 = \pi\varepsilon^2(1-\gamma_\beta)\beta f p(\widehat{x}) + \underbrace{\int_{B_\varepsilon}(1-\gamma_\beta)\beta f[p - p(\widehat{x})]}_{\mathcal{E}_{17}(\varepsilon)}. \tag{A56}$$

with remainders $\mathcal{E}_{15}(\varepsilon)$, $\mathcal{E}_{16}(\varepsilon)$, and $\mathcal{E}_{17}(\varepsilon)$ bounded as follows:

$$|\mathcal{E}_{15}(\varepsilon)| \leqslant \varepsilon\|u_\varepsilon - u\|_{L^2(\Omega)} = o(\varepsilon^2), \tag{A57}$$

$$|\mathcal{E}_{16}(\varepsilon)| \leqslant \varepsilon\|x-\widehat{x}\|_{L^2(B_\varepsilon)} = o(\varepsilon^2), \tag{A58}$$

$$|\mathcal{E}_{17}(\varepsilon)| \leqslant \varepsilon\|x-\widehat{x}\|_{L^2(B_\varepsilon)} = o(\varepsilon^2), \tag{A59}$$

where we have used Corollary A1 and the interior elliptic regularity of functions u and p. The integrals B_6 and B_7 can be developed in the following way,

$$B_6 + B_7 = \underbrace{\int_{B_\varepsilon}(1-\gamma_\alpha)\alpha\sigma(u)\cdot\nabla^s p}_{B_9} + \underbrace{\int_{B_\varepsilon}(1-\gamma_\alpha)\alpha\sigma(w_\varepsilon)\cdot\nabla^s p}_{B_{10}} + \underbrace{\int_{B_\varepsilon}(1-\gamma_\alpha)\alpha\sigma(\widetilde{u}_\varepsilon)\cdot\nabla^s p}_{\mathcal{E}_{18}(\varepsilon)}, \tag{A60}$$

where we have introduced the ansatz (A1). Therefore,

$$B_9 \quad = \quad \pi\varepsilon^2(1-\gamma_\alpha)\alpha\sigma(u)\cdot\nabla^s p(\widehat{x}) + \underbrace{\int_{B_\varepsilon}(1-\gamma_\alpha)\alpha[\sigma(u)\cdot\nabla^s p - \sigma(u)\cdot\nabla^s p(\widehat{x})]}_{\mathcal{E}_{19}(\varepsilon)}. \quad \text{(A61)}$$

with remainders $\mathcal{E}_{18}(\varepsilon)$ and $\mathcal{E}_{19}(\varepsilon)$, bounded as follows:

$$|\mathcal{E}_{18}(\varepsilon)| \quad \leqslant \quad \varepsilon\|\widetilde{u}_\varepsilon\|_{H^1(\Omega)} = o(\varepsilon^2), \quad \text{(A62)}$$

$$|\mathcal{E}_{19}(\varepsilon)| \quad \leqslant \quad \varepsilon\|\widetilde{u}_\varepsilon\|_{H^1(\Omega)} = o(\varepsilon^2), \quad \text{(A63)}$$

where we have used Lemma A1 together with the interior elliptic regularity of functions u and p. The last integral B_{11} can be rewritten as

$$B_{11} \quad = \quad \pi\varepsilon^2(1-\gamma_\alpha)\alpha\mathbb{P}\sigma(u)\cdot\nabla^s p(\widehat{x}) + \underbrace{\int_{B_\varepsilon}(1-\gamma_\alpha)\alpha\sigma(w_\varepsilon)\cdot\nabla^s(p - p(\widehat{x}))}_{\mathcal{E}_{20}(\varepsilon)}, \quad \text{(A64)}$$

where we have used the explicit solution (A6)–(A8). The remainders $\mathcal{E}_{20}(\varepsilon)$ can be bounded as follows:

$$|\mathcal{E}_{20}(\varepsilon)| \quad \leqslant \quad C_1\|\sigma(w_\varepsilon)\|_{L^2(B_\varepsilon)}\|x-\widehat{x}\|_{L^2(B_\varepsilon)} = o(\varepsilon^2). \quad \text{(A65)}$$

Finally, after collecting the obtained results, we have

$$\mathcal{J}_\varepsilon(u_\varepsilon) - \mathcal{J}(u) = -\pi\varepsilon^2[2\alpha\mathbb{P}\sigma(u)\cdot\nabla^s(u+p)(\widehat{x}) + (1-\gamma_\rho)\rho k u p(\widehat{x}) - (1-\gamma_\beta)\beta f p(\widehat{x})] + \sum_{i=11}^{20}\mathcal{E}_i(\varepsilon), \quad \text{(A66)}$$

where the remainders $\mathcal{E}_i(\varepsilon) = o(\varepsilon^2)$, for $i = 11\cdots 20$. □

References

1. Masur, E.F.; Mroz, Z. Non-stationary optimality conditions in structural design. *Int. J. Solids Struct.* **1979**, *15*, 503–512. [CrossRef]
2. Haug, E.J.; Rousselet, B. Design sensitivity analysis in structural mechanics. II. eigenvalue variationsi. *J. Struct. Mech.* **1979**, *8*, 161–186. [CrossRef]
3. Seyranian, A.P.; Lund, E.; Olhoff, N. Multiple eigenvalues in structural optimization problems. *Struct. Optim.* **1994**, *8*, 207–227. [CrossRef]
4. Jensen, J.S.; Pedersen, N.L. On maximal eigenfrequency separation in two-material structures: The 1D and 2D scalar cases. *J. Sound Vib.* **2006**, *289*, 967–986. [CrossRef]
5. Gravesen, J.; Evgrafov, A.; Nguyen, D.M. On the sensitivities of multiple eigenvalues. *Struct Multidiscip Optim* **2011**, *44*, 583–587. [CrossRef]
6. Torii, A.; Faria, J.R. Structural optimization considering smallest magnitude eigenvalues: A smooth approximation. *J. Braz. Soc. Mech. Sci. Eng.* **2017**, *39*, 1745–1754. [CrossRef]
7. Ammari, H.; Khelifi, A. Electromagnetic scattering by small dielectric inhomogeneities. *J. Math. Pures Appl.* **2003**, *82*, 749–842. [CrossRef]
8. Nazarov, S.A.; Sokołowski, J. Spectral problems in the shape optimisation. Singular boundary perturbations. *Asymptot. Anal.* **2008**, *56*, 159–204.
9. Amstutz, S. Augmented Lagrangian for cone constrained topology optimization. *Comput. Optim. Appl.* **2011**, 101–122.. [CrossRef]
10. Carvalho, F.; Ruscheinsky, D.; Giusti, S.; Anflor, C.; Novotny, A. Topological Derivative-Based Topology Optimization of Plate Structures Under Bending Effects. *Struct. Multidiscip. Optim.* **2020**, *63*, 617–630. [CrossRef]
11. Ruscheinsky, D.; Carvalho, F.S.; Anflor, C.; Novotny, A.A. Topological asymptotic analysis of a diffusive–convective–reactive problem. *Eng. Comput.* **2020**. [CrossRef]
12. Takezawa, A.; Nishiwaki, S.; Kitamura, M. Shape and topology optimization based on the phase field method and sensitivity analysis. *J. Comput. Phys.* **2010**, *229*, 2697–2718. [CrossRef]
13. Qian, M.; Hu, X.; Zhu, S. A phase field method based on multi-level correction for eigenvalue topology optimization. *Comput. Methods Appl. Mech. Eng.* **2022**, *401*, 115646. [CrossRef]

14. Amstutz, S.; Andrä, H. A new algorithm for topology optimization using a level-set method. *J. Comput. Phys.* **2006**, *216*, 573–588. [CrossRef]
15. Novotny, A.A.; Sokołowski, J. *Topological Derivatives in Shape Optimization*; Interaction of Mechanics and Mathematics; Springer: Berlin/Heidelberg, Germany, 2013; p. 324.
16. Novotny, A.A.; Sokolowski, J. *An Introdution to the Topological Derivative Method*; Springer Briefs in Mathematics; Springer: New York, NY, USA, 2020.

Disclaimer/Publisher's Note: The statements, opinions and data contained in all publications are solely those of the individual author(s) and contributor(s) and not of MDPI and/or the editor(s). MDPI and/or the editor(s) disclaim responsibility for any injury to people or property resulting from any ideas, methods, instructions or products referred to in the content.